Navier–Stokes/Forchheimer models for filtration through porous media

F. Cimolin [a], M. Discacciati [b,*]

[a] *Politecnico di Torino, Corso Duca degli Abruzzi 24, I-10129 Torino, Italy*
[b] *Laboratori de Càlcul Numèric (LaCàN), Departament de Matemàtica Aplicada III (MA3), Universitat Politècnica de Catalunya (UPC BarcelonaTech), Campus Nord UPC – C2, E-08034 Barcelona, Spain*

A B S T R A C T

Modeling the filtration of incompressible fluids through porous media requires dealing with different types of partial differential equations in the fluid and porous subregions of the computational domain. Such equations must be coupled through physically significant continuity conditions at the interface separating the two subdomains. To avoid the difficulties of this heterogeneous approach, a widely used strategy is to consider the Navier–Stokes equations in the whole domain and to correct them introducing suitable terms that mimic the presence of the porous medium. In this paper we discuss these two different methodologies and we compare them numerically on a sample test case after proposing an iterative algorithm to solve a Navier–Stokes/Forchheimer problem. Finally, we apply these strategies to a problem of internal ventilation of motorbike helmets.

1. Introduction

In this paper we consider the modeling and numerical simulation of incompressible fluid flows in regions partially occupied by porous media. The driving motivation of this work comes from a specific industrial problem of internal ventilation for motorcycle helmets. However, problems associated with filtration of fluids in porous media have many other applications from geophysics to engineering and also physiology. Consider for example the percolation of water in hydrological basins through rocks or sand, the filtration of biofluids through living tissues, as well as industrial processes involving fluids going through filters and foams.

The problem of industrial interest discussed in this work, which will be precisely described in Section 5, consists in modeling and simulating the internal air flow of a motorcycle helmet. A series of intakes and outtakes connected by channels dug into the protection layer let the fresh air enter the helmet and filtrate through the comfort tissue and the hair of the rider. An appropriate ventilation capable of effectively removing the heat and moisture produced by the head must be guaranteed in order to preserve the safety of the rider even in very hot and humid climates.

This work, which focuses only on the fluid-dynamics aspects of the air flow, aims at investigating the possible modeling approaches for the physical description of the system, and it represents a preliminary step towards a more complex model taking into account heat and sweat-related phenomena too (see [11]). In spite of the specific application, most of the considerations associated with both modeling and numerical simulation that will be discussed throughout the paper are valid in the more general framework of flow over saturated porous media.

* Corresponding author. Tel.: +34 93 401 0894; fax: +34 93 401 1825.
E-mail addresses: flavio.cimolin@polito.it (F. Cimolin), marco.discacciati@upc.edu (M. Discacciati).

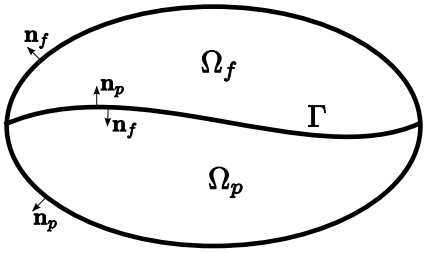

Fig. 1. Subdivision of the computational domain Ω in a fluid region Ω_f and a porous domain Ω_p.

Due to the physical heterogeneity of the domain, a correct physical modeling of filtration processes would require to introduce different systems of partial differential equations in the free fluid domain and in the porous medium region, giving rise to a heterogeneous differential system.

While for the vast majority of applications the Navier–Stokes equations represent the model to describe incompressible flows in the free-fluid region, the modeling of flows through a saturated porous medium may require different models depending on the characteristics of the porous medium itself. A classical model is given by the Darcy law [18], the simplest linear relation between the velocity and the pressure. However, in case of high permeabilities the non-linear Forchheimer equation [25] is usually adopted.

A crucial issue in the definition of these heterogeneous models is the choice of suitable coupling conditions to describe the fluid flow across the surface of the porous medium through which the filtration occurs.

Those coupled problems have received an increasing attention during the last years from both the mathematical and the numerical point of view. Starting from the original experimental works of Beavers and Joseph on the coupling conditions between a fluid and a porous medium, mathematical investigations have been carried out in [22,36–38,41,42]. Under those conditions, the analysis of a coupled Stokes/Darcy problem has been studied in [10,17,19,20,28,29,26,27,30,40,48] in the steady case, and in [12,53] in the time-dependent case. Moreover, the case of the Navier–Stokes equations has been considered in [3,14,19,31].

However, because of the difficulties associated to the set-up and implementation of those models, a different approach is widely used in many practical applications and it is implemented in most commercial softwares. This method, often called penalization approach (see, e.g., [9,34,35,39]), consists in considering in the whole computational domain a modified formulation of the Navier–Stokes equations which reduce to their classical form in the fluid region while they include additional resistance terms in the porous region. This approach is similar to the so-called fictitious domain method [1,39].

In this paper we compare these two different techniques studying their mathematical formulation and their finite element approximation. In particular, the paper is organized as follows. In Section 2, we present the differential models for the fluid flow as well as for the saturated porous media flow, we discuss the coupling conditions for the heterogeneous case and we introduce suitable adimensional formulations. In Section 3, we consider the numerical approximation and we introduce possible solution strategies for the space–time discretization of these problems. Numerical results for the heterogeneous Navier–Stokes/Forchheimer model are presented in Section 4, which includes also a comparison of the simulation results obtained by the other modeling approaches. Finally, in Section 5 we show an example of application of the penalization method to the problem of internal ventilation of a helmet.

2. Mathematical models for the flow over a porous medium

We consider a bounded domain $\Omega \subset \mathbb{R}^d$ $(d = 2, 3)$ partitioned into two non-overlapping regions: $\overline{\Omega} = \overline{\Omega}_f \cup \overline{\Omega}_p$, $\Omega_f \cap \Omega_p = \emptyset$, where Ω_f is the fluid domain (for example occupied by air or water) and Ω_p the saturated porous medium domain. We indicate by $\Gamma = \overline{\Omega}_f \cap \overline{\Omega}_p$ the interface between the two domains (see Fig. 1). From the physical point of view, Γ represents the contact surface between the porous medium and the free fluid.

2.1. Fluid domain: the Navier–Stokes equations

In the fluid region Ω_f, we consider a confined incompressible viscous fluid modeled by the Navier–Stokes equations: for all $t > 0$,

$$\begin{aligned} &\rho\left(\frac{\partial \mathbf{u}_f}{\partial t} + (\mathbf{u}_f \cdot \nabla)\mathbf{u}_f\right) - \mu \Delta \mathbf{u}_f + \nabla p_f = \mathbf{0} \quad \text{in } \Omega_f, \\ &\nabla \cdot \mathbf{u}_f = 0 \qquad\qquad\qquad\qquad\qquad\quad \text{in } \Omega_f, \end{aligned} \tag{1}$$

where $\mathbf{u}_f$ and p_f denote respectively the velocity and the pressure of the fluid, ρ and μ are respectively the density and dynamic viscosity of the fluid and we assume that no external body forces are applied.

We have denoted by ∇, $\nabla\cdot$ and Δ, respectively, the gradient, the divergence and the Laplace operators with respect to the space coordinates. Moreover, we recall that $(\mathbf{v}\cdot\nabla)\mathbf{w} = \sum_{i=1}^{d} v_i \frac{\partial \mathbf{w}}{\partial x_i}$ for all vector functions $\mathbf{v} = (v_1, \ldots, v_d)$, $\mathbf{w} = (w_1, \ldots, w_d)$.

The Navier–Stokes equations are well-suited to numerically simulate laminar flows for which the Reynolds number

$$\mathrm{Re}_f = \frac{\rho U L}{\mu} \tag{2}$$

is not too high, U and L being a characteristic velocity and a characteristic length scale of the problem, respectively. For high Reynolds numbers turbulence effects become important and the Navier–Stokes equations need to be augmented with turbulence models, such as the RANS (Reynolds Averaged Navier–Stokes) ones. In our applications we will always place ourselves in the laminar case.

2.2. Filtration through the porous domain

Filtration through a saturated porous domain can be modeled by the Darcy law, which introduces an average fluid velocity on sample volumes of the porous medium sufficiently large with respect to the pore size.

The Darcy law is the simplest (linear) relation between the seepage velocity $\mathbf{u}_p$ and the pressure p_p in the porous medium, and it states that

$$\mathbf{u}_p = -\frac{K}{\mu}\nabla p_p \quad \text{in } \Omega_p, \tag{3}$$

where μ is the dynamic viscosity coefficient already defined in (1), while K is the permeability coefficient. This law was originally obtained by Darcy with a famous experiment [18], and later rigorously derived from the Navier–Stokes equations by mathematical homogenization on structured porous grids (see, e.g., [50]). The permeability coefficient K can assume values ranging from $K = 10^{-5}$ m^2 for very porous artificial materials to $K = 10^{-20}$ m^2 for particular kinds of soils or rocks. In case of a non-isotropic medium the scalar coefficient K is substituted by a permeability tensor $\mathbf{K}$.

As the seepage velocity increases, the transition towards a non-linear drag is quite smooth. In order to characterize the importance of the inertial effects, similarly to the Navier–Stokes equations, it is possible to define the Reynolds number associated to the pores

$$\mathrm{Re}_p = \frac{\rho U \delta}{\mu}, \tag{4}$$

where δ is the characteristic pore size.

The Darcy law is reliable for values of $\mathrm{Re}_p < 1$ (see, e.g., [4]), otherwise it is necessary to consider a more general model which can account also for the inertial effects, like the non-linear Forchheimer equation [25]:

$$\nabla p_p = -\frac{\mu}{K}\mathbf{u}_p - \frac{\rho C_F}{\sqrt{K}}|\mathbf{u}_p|\mathbf{u}_p \quad \text{in } \Omega_p, \tag{5}$$

where C_F is the inertial resistance coefficient (or tensor in the non-isotropic case). The transition between the Darcy and the Forchheimer regimes occurs in the range $1 < \mathrm{Re}_p < 10$. More in general, non-linear correction terms of the form $|\mathbf{u}_p|^\alpha \mathbf{u}_p$ with $1 \leqslant \alpha \leqslant 2$ can be considered for Darcy's law. Detailed discussions about their physical interpretation can be found in [23,43]. As the Darcy law, the Forchheimer equation can be derived by homogenization from the Navier–Stokes equations (see [15]).

The filtration model is fully determined considering the continuity equation:

$$\nabla \cdot \mathbf{u}_p = 0 \quad \text{in } \Omega_p. \tag{6}$$

The latter, combined with the Darcy equation (3), leads to the following elliptic equation involving only the pressure:

$$-\nabla \cdot \left(\frac{K}{\mu}\nabla p_p\right) = 0 \quad \text{in } \Omega_p. \tag{7}$$

If only (7) is solved in Ω_p, then the velocity can be recovered using the Darcy law (3).

2.3. Coupling conditions across the interface

To represent the filtration of the free fluid through the porous medium, we have to introduce suitable coupling conditions between the Navier–Stokes and Darcy (or Forchheimer) equations across their common interface Γ. In particular, we consider the following three conditions.

1. Continuity of the normal component of the velocity:

$$\mathbf{u}_f \cdot \mathbf{n}_f = -\mathbf{u}_p \cdot \mathbf{n}_p \quad \text{on } \Gamma, \tag{8}$$

where $\mathbf{n}_f$ and $\mathbf{n}_p$ are the unit normal vectors external to $\partial\Omega_f$ and $\partial\Omega_p$, respectively (see Fig. 1). Notice that $\mathbf{n}_f = -\mathbf{n}_p$ on Γ. Using Darcy law (3), Eq. (8) can be rewritten as

$$\mathbf{u}_f \cdot \mathbf{n}_f = \frac{K}{\mu}\frac{\partial p_p}{\partial n_p} \quad \text{on } \Gamma. \tag{9}$$

This condition is a consequence of the incompressibility of the fluid.

2. Continuity of the normal stresses across Γ (see, e.g., [36]):

$$p_f - \mu\frac{\partial \mathbf{u}_f}{\partial n_f}\cdot\mathbf{n}_f = p_p \quad \text{on } \Gamma. \tag{10}$$

Remark that pressures may be discontinuous across the interface.

3. Finally, in order to have a completely determined flow in the free-fluid region, we have to specify a further condition on the tangential component of the fluid velocity at the interface.
Beavers and Joseph [5] proposed an experimental condition stating that the difference between the slip velocity and the tangential seepage velocity at the interface is proportional to the shear rate therein:

$$-\left(\frac{\partial \mathbf{u}_f}{\partial n_f}\right)_\tau = \frac{\alpha_{BJ}}{\sqrt{K}}(\mathbf{u}_f - \mathbf{u}_p)_\tau \quad \text{on } \Gamma. \tag{11}$$

By $(\mathbf{v})_\tau$ we indicate the tangential component to the interface of the vector $\mathbf{v}$:

$$(\mathbf{v})_\tau = \mathbf{v} - \mathbf{v}\cdot\mathbf{n} \quad \text{on } \Gamma. \tag{12}$$

The constant α_{BJ} usually assumes values between 0.8 and 1.2 (see [5]).
Since the seepage velocity $\mathbf{u}_p$ is far smaller than the fluid slip velocity $\mathbf{u}_f$ at the interface, Saffman proposed to use the following simplified condition (the so-called Beavers–Joseph–Saffman condition) [49]:

$$-\left(\frac{\partial \mathbf{u}_f}{\partial n_f}\right)_\tau = \frac{\alpha_{BJ}}{\sqrt{K}}(\mathbf{u}_f)_\tau \quad \text{on } \Gamma. \tag{13}$$

This condition was later derived mathematically by homogenization by Jäger and Mikelić [36–38].

The three coupling conditions described in this section have been extensively studied and analyzed also in [20,21,40,45,48,51].

Remark 2.1. Notice that we have written the Navier–Stokes equations in time-dependent form, while we consider steady models for the flow in the porous medium. This can be justified by the fact that the velocity in the fluid domain is generally much higher than the seepage velocity, so that the latter can be treated as steady at least during small time intervals. If this assumption was not satisfied, it would be possible to consider an unsteady model also in Ω_p as studied for example in [12].

2.4. Penalization method

The coupled model discussed in the above sections is quite complex to solve, mainly because of the intrinsic difference in nature between the equations in the subdomains Ω_f and Ω_p. For this reason, the so-called penalization approach has been introduced to model the flow over porous media (see, e.g., [9,34,35]). This method consists in considering a modified set of Navier–Stokes equations in the whole domain including two penalization terms associated to the resistance induced by the porous medium in the subregion Ω_p. These terms are related to the linear Darcy and the non-linear Forchheimer equations (3) and (5).

More precisely, we consider the momentum equation:

$$\rho\left(\frac{\partial \mathbf{u}}{\partial t} + (\mathbf{u}\cdot\nabla)\mathbf{u}\right) - \mu\Delta\mathbf{u} + \nabla p + \left(\frac{\mu}{K}\mathbf{u} + \frac{\rho C_F}{\sqrt{K}}|\mathbf{u}|\mathbf{u}\right)\chi_{\Omega_p} = \mathbf{0} \quad \text{in } \Omega, \tag{14}$$

where the physical constants are the same already introduced in (1) and (5), while $\chi_{\Omega_p} = 1$ in Ω_p and $\chi_{\Omega_p} = 0$ elsewhere, so that the last two terms vanish in the fluid domain. The variable $\mathbf{u}$ corresponds to the real velocity in Ω_f and to the seepage velocity in Ω_p.

Remark 2.2. Notice that this method can be enhanced to deal with inner solid regions too, following the so-called "fictitious domain" approach proposed in [39]: the modified Navier–Stokes equations are solved in the whole domain, with very strong variations of the permeability coefficient. Indeed, it can be rigorously shown via homogenization techniques (see [1]) that the proposed approach is consistent with the modeling of both solid ($K \to 0$) and fluid ($K \to +\infty$) regions.

Concerning the physical meaning of (14), the diffusive contribution $-\mu\Delta\mathbf{u}$ has been shown to be consistent with the modeling of highly porous materials, such as, for example, synthetic foams with porosity greater than 0.6, and sometimes it is referred to as Brinkman [8], or Brinkman–Forchheimer equation [52], possibly with $\tilde{\mu} \neq \mu$. On the other hand, the non-linear convective term $(\mathbf{u}\cdot\nabla)\mathbf{u}$ has been criticized as an unsatisfactory way to include non-linear inertial effects, since, for example, it vanishes even for a steady incompressible unidirectional flow, regardless of the magnitude of the velocity $\mathbf{u}$.

However, since the penalization method is much easier to implement than the coupled approach of Sections 2.1–2.3, it is widely used in commercial softwares. Indeed, most of the commercial packages capable of simulating flows in domains partially occupied by porous media are based on this approach (see, e.g., [13,2,24]). In these codes, the porous medium is usually characterized by two constants P_v and P_i called, respectively, *viscous* and *inertial resistance* which are different from zero only in the porous domain Ω_p. Then, the following penalized Navier–Stokes equations are solved:

$$\begin{aligned} &\rho\left(\frac{\partial\mathbf{u}}{\partial t}+(\mathbf{u}\cdot\nabla)\mathbf{u}\right)-\mu\Delta\mathbf{u}+\nabla p+P_v\mathbf{u}+P_i|\mathbf{u}|\mathbf{u}=\mathbf{0} \quad \text{in } \Omega,\\ &\nabla\cdot\mathbf{u}=0 \qquad\qquad\qquad\qquad\qquad\qquad\qquad\qquad\qquad\quad \text{in } \Omega, \end{aligned} \tag{15}$$

where

$$P_v=\begin{cases}0 & \text{in } \Omega_f\\ \mu/K & \text{in } \Omega_p,\end{cases} \quad \text{and} \quad P_i=\begin{cases}0 & \text{in } \Omega_f\\ \rho C_F/\sqrt{K} & \text{in } \Omega_p.\end{cases} \tag{16}$$

2.5. Dimensionless formulations

To better compare the models that we have considered, we introduce their dimensionless forms. We define the following dimensionless variables:

$$\mathbf{x}'=\frac{\mathbf{x}}{L}, \qquad t'=\frac{U}{L}t, \qquad \mathbf{u}'_f=\frac{\mathbf{u}_f}{U}, \qquad \mathbf{u}'_p=\frac{\mathbf{u}_p}{U}, \qquad p'_f=\frac{p_f}{\rho U^2}, \qquad p'_p=\frac{p_p}{\rho U^2}, \tag{17}$$

where L and U are respectively a characteristic length and velocity for the problem (we use the same for both the fluid and the porous medium).

By substituting (17) in (1) we obtain the dimensionless formulation of the Navier–Stokes equations:

$$\begin{aligned} &\frac{\partial\mathbf{u}'_f}{\partial t'}+\left(\mathbf{u}'_f\cdot\nabla\right)\mathbf{u}'_f-\frac{1}{\mathrm{Re}_f}\Delta\mathbf{u}'_f+\nabla p'_f=\mathbf{0} \quad \text{in } \Omega_f,\\ &\nabla\cdot\mathbf{u}'_f=0 \qquad\qquad\qquad\qquad\qquad\qquad\qquad\quad \text{in } \Omega_f, \end{aligned} \tag{18}$$

where Re_f is the Reynolds number defined in (2).

The dimensionless form of the Darcy law (3) becomes

$$\mathbf{u}'_p=-\,\mathrm{Gr}_n\,\nabla p'_p \quad \text{in } \Omega_p, \tag{19}$$

where the dimensionless group Gr_n is defined as

$$\mathrm{Gr}_n=\frac{\rho KU}{\mu L}. \tag{20}$$

On the other hand, the dimensionless form of the Forchheimer equation (5) reads:

$$\mathbf{u}'_p+\mathrm{Gr}_f\left|\mathbf{u}'_p\right|\mathbf{u}'_p=-\,\mathrm{Gr}_n\,\nabla p'_p \quad \text{in } \Omega_p, \tag{21}$$

having denoted by Gr_f the dimensionless group

$$\mathrm{Gr}_f=\frac{\rho C_F U\sqrt{K}}{\mu}. \tag{22}$$

The three coupling conditions (9), (10), (13) at the interface are made dimensionless too, obtaining

$$\mathbf{u}'_f\cdot\mathbf{n}_f=\mathrm{Gr}_n\,\frac{\partial p'_p}{\partial n'_p}, \tag{23}$$

$$p'_f-\frac{1}{\mathrm{Re}_f}\frac{\partial\mathbf{u}'_f}{\partial n'_f}\cdot\mathbf{n}_f=p'_p, \tag{24}$$

$$-\left(\frac{\partial\mathbf{u}'_f}{\partial n'_f}\right)_\tau=\mathrm{Gr}_c\left(\mathbf{u}'_f\right)_\tau, \tag{25}$$

where Gr_c is defined by

$$\mathrm{Gr}_c = \frac{\alpha_{BJ} L}{\sqrt{K}}. \tag{26}$$

Finally, the dimensionless form of the penalized Navier–Stokes equations (15) becomes

$$\frac{\partial \mathbf{u}'}{\partial t'} + (\mathbf{u}' \cdot \nabla)\mathbf{u}' - \frac{1}{\mathrm{Re}} \Delta \mathbf{u}' + \nabla p' + \mathrm{Gr}_v \, \mathbf{u}' + \mathrm{Gr}_i |\mathbf{u}'| \mathbf{u}' = \mathbf{0} \quad \text{in } \Omega, \tag{27}$$

with dimensionless groups

$$\mathrm{Re} = \frac{\rho L U}{\mu}, \qquad \mathrm{Gr}_v = \frac{P_v L}{\rho U}, \qquad \mathrm{Gr}_i = \frac{P_i L}{\rho}. \tag{28}$$

In the following we will refer to the dimensionless formulations omitting the apices for simplicity of notation. For the sake of clarity, let us summarize the models that we will consider in the next sections.

- *Navier–Stokes/Darcy (NSD) model*:

$$\begin{aligned}
&\frac{\partial \mathbf{u}_f}{\partial t} + (\mathbf{u}_f \cdot \nabla)\mathbf{u}_f - \frac{1}{\mathrm{Re}_f} \Delta \mathbf{u}_f + \nabla p_f = \mathbf{0} && \text{in } \Omega_f, \\
&\nabla \cdot \mathbf{u}_f = 0 && \text{in } \Omega_f, \\
&-\nabla \cdot (\mathrm{Gr}_n \nabla p_p) = 0 && \text{in } \Omega_p, \\
&\mathbf{u}_f \cdot \mathbf{n}_f = \mathrm{Gr}_n \frac{\partial p_p}{\partial n_p} && \text{on } \Gamma, \\
&p_f - \frac{1}{\mathrm{Re}_f} \frac{\partial \mathbf{u}_f}{\partial n_f} \cdot \mathbf{n}_f = p_p && \text{on } \Gamma, \\
&-\left(\frac{\partial \mathbf{u}_f}{\partial n_f} \right)_\tau = \mathrm{Gr}_c \, (\mathbf{u}_f)_\tau && \text{on } \Gamma.
\end{aligned} \tag{29}$$

- *Navier–Stokes/Forchheimer (NSF) model*:

$$\begin{aligned}
&\frac{\partial \mathbf{u}_f}{\partial t} + (\mathbf{u}_f \cdot \nabla)\mathbf{u}_f - \frac{1}{\mathrm{Re}_f} \Delta \mathbf{u}_f + \nabla p_f = \mathbf{0} && \text{in } \Omega_f, \\
&\nabla \cdot \mathbf{u}_f = 0 && \text{in } \Omega_f, \\
&\mathbf{u}_p + \mathrm{Gr}_f \, |\mathbf{u}_p| \mathbf{u}_p = -\mathrm{Gr}_n \nabla p_p = 0 && \text{in } \Omega_p, \\
&\nabla \cdot \mathbf{u}_p = 0 && \text{in } \Omega_p, \\
&\mathbf{u}_f \cdot \mathbf{n}_f = -\mathbf{u}_p \cdot \mathbf{n}_p && \text{on } \Gamma, \\
&p_f - \frac{1}{\mathrm{Re}_f} \frac{\partial \mathbf{u}_f}{\partial n_f} \cdot \mathbf{n}_f = p_p && \text{on } \Gamma, \\
&-\left(\frac{\partial \mathbf{u}_f}{\partial n_f} \right)_\tau = \mathrm{Gr}_c \, (\mathbf{u}_f)_\tau && \text{on } \Gamma.
\end{aligned} \tag{30}$$

- *Penalization (PE) model*:

$$\begin{aligned}
&\frac{\partial \mathbf{u}}{\partial t} + (\mathbf{u} \cdot \nabla)\mathbf{u} - \frac{1}{\mathrm{Re}} \Delta \mathbf{u} + \nabla p + \mathrm{Gr}_v \, \mathbf{u} + \mathrm{Gr}_i \, |\mathbf{u}| \mathbf{u} = \mathbf{0} && \text{in } \Omega, \\
&\nabla \cdot \mathbf{u} = 0 && \text{in } \Omega.
\end{aligned} \tag{31}$$

All the physical variables are dimensionless. Suitable boundary conditions will be introduced in Section 2.6.

2.6. Boundary conditions

We set now the boundary conditions referring, for simplicity to a specific 2D problem, but what we present can be extended to more general settings.

We consider the setting in Fig. 2, in which a horizontal fluid flows upon a saturated porous medium. The flow enters from the fluid inlet γ_1 and exits at both the fluid and porous outlets γ_3 and δ_3. All the other boundaries are impermeable,

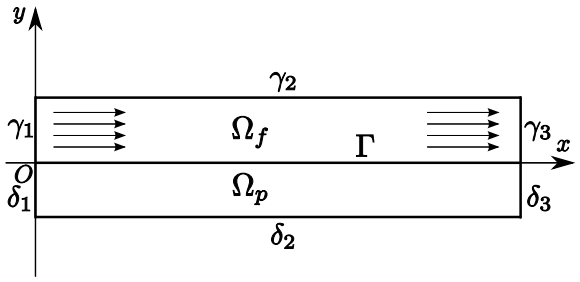

Fig. 2. Scheme of the bidimensional sample problem.

with no-slip condition on γ_2 and with a slip condition on δ_1 and δ_2. As reference dimensionless parameters we consider L as the height of the fluid channel and U as the maximal velocity at the inlet.

More precisely, the boundary conditions that we use for the NSD model (29) read:

$$\begin{aligned}
&\mathbf{u}_f = \mathbf{u}_{pois} && \text{on } \gamma_1,\\
&\mathbf{u}_f = \mathbf{0} && \text{on } \gamma_2,\\
&p_f \mathbf{n}_f - \frac{1}{\mathrm{Re}_f}\frac{\partial \mathbf{u}_f}{\partial n_f} = \mathbf{0} && \text{on } \gamma_3,\\
&\frac{\partial p_p}{\partial n_p} = 0 && \text{on } \delta_1 \cup \delta_2,\\
&p_p = 0 && \text{on } \delta_3.
\end{aligned} \tag{32}$$

The function $\mathbf{u}_{pois}$ is a given Pouiseuille velocity profile on γ_1. The same boundary conditions apply for the NSF problem (30) with $(32)_4$ replaced by

$$\mathbf{u}_p \cdot \mathbf{n}_p = 0 \quad \text{on } \delta_1 \cup \delta_2.$$

For the PE problem (31), we have to impose a slightly different set of boundary conditions:

$$\begin{aligned}
&\mathbf{u} = \mathbf{u}_{pois} && \text{on } \gamma_1,\\
&\mathbf{u} = \mathbf{0} && \text{on } \gamma_2,\\
&p\mathbf{n} - \frac{1}{\mathrm{Re}}\frac{\partial \mathbf{u}}{\partial n} = \mathbf{0} && \text{on } \gamma_3,\\
&\mathbf{u} \cdot \mathbf{n} = 0 && \text{on } \delta_1 \cup \delta_2,\\
&\left(\frac{\partial \mathbf{u}}{\partial n}\right)_\tau = 0 && \text{on } \delta_1 \cup \delta_2,\\
&p\mathbf{n} - \frac{1}{\mathrm{Re}}\frac{\partial \mathbf{u}}{\partial n} = \mathbf{0} && \text{on } \delta_3.
\end{aligned} \tag{33}$$

Notice that condition $(32)_5$ has been replaced by $(33)_6$ since in the latter case the stress on δ_3 is not given by the sole pressure, but by the whole Cauchy stress tensor. Moreover, condition $(32)_4$ has been changed into $(33)_4$ and $(33)_5$. Indeed, thanks to Darcy's law, $(32)_4$ corresponds to the null normal velocity condition $(33)_4$, while $(33)_5$ has been introduced to ensure the well-posedness of the problem.

As initial condition for all models we assume the velocity in the fluid region Ω_f to be equal to the Poiseuille flow profile at the initial time, i.e., $\mathbf{u}_f(t=0) = \mathbf{u}_{pois}$ in Ω_f. On the other hand, we assume that at the initial time there is no flow in the porous medium, and that at the beginning of the simulation a rigid impermeable device separating the two domains is suddenly removed, allowing the penetration of the fluid in the porous bed.

3. Numerical approximation and solution algorithms

In this section we address the finite element approximation of the coupled problems considered in Sections 2.5–2.6 and we propose an iterative solution method based on a domain decomposition approach.

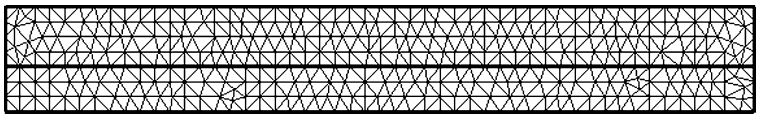

Fig. 3. Example of regular compatible computational mesh.

3.1. Space discretization

We consider a regular triangulation $\mathcal{T}_h$ of the domain $\overline{\Omega}_f \cup \overline{\Omega}_p$, depending on a positive parameter $h > 0$, made up of triangles T. We assume that the triangulations $\mathcal{T}_{fh}$ and $\mathcal{T}_{ph}$ induced on the subdomains Ω_f and Ω_p are compatible on Γ, that is they share the same edges therein. Finally, we suppose the triangulation induced on Γ to be quasi-uniform (see, e.g., [46]). An example of regular compatible triangulation is shown in Fig. 3.

Several choices of finite element spaces can be made. If we indicate by $\mathbf{W}_h$ and Q_h the finite element spaces which approximate the velocity and pressure fields, respectively, for the Navier–Stokes problem or for the penalization model, there must exist a positive constant $\beta^* > 0$, independent of h, such that the classical inf–sup condition is satisfied, i.e., $\forall q_h \in Q_h$, $\exists \mathbf{v}_h \in \mathbf{W}_h$, $\mathbf{v}_h \neq \mathbf{0}$, such that

$$\int_{\mathcal{D}} q_h \nabla \cdot \mathbf{v}_h \geqslant \beta^* \|\mathbf{v}_h\|_{H^1(\mathcal{D})} \|q_h\|_{L^2(\mathcal{D})},$$

where $\mathcal{D} = \Omega_f$ for (29) and (30) and $\mathcal{D} = \Omega$ for (31).

Several families of finite element spaces satisfying the inf–sup condition are provided in [7]. In the following, for the sake of exposition, we will make the special choice of piecewise quadratic elements for the velocity and piecewise linear for the pressure.

More precisely, we start by defining the following discrete spaces for the NSD problem:

$$\begin{aligned}
&\mathbf{X}_{fh} = \left\{\mathbf{v}_h \in \mathcal{C}^0(\overline{\Omega}_f)\colon\ \mathbf{v}_{h|T} \in \left[\mathbb{P}_2(T)\right]^2\ \forall T \in \mathcal{T}_{fh}\right\},\\
&\mathbf{V}_{fh} = \{\mathbf{v}_h \in \mathbf{X}_{fh}\colon\ \mathbf{v}_h = \mathbf{0} \text{ on } \gamma_1 \cup \gamma_2\},\\
&Q_{fh} = \left\{q_h \in \mathcal{C}^0(\overline{\Omega}_f)\colon\ q_{h|T} \in \mathbb{P}_1(T)\ \forall T \in \mathcal{T}_{fh}\right\},\\
&W_{ph} = \left\{q_h \in \mathcal{C}^0(\overline{\Omega}_p)\colon\ q_{h|T} \in \mathbb{P}_2(T)\ \forall T \in \mathcal{T}_{ph},\ q_h = 0 \text{ on } \delta_3\right\}.
\end{aligned}$$

Then, the Galerkin approximation of the coupled NSD problem (29) reads: find $\mathbf{u}_{fh}(t) \in \mathbf{X}_{fh}$, $p_{fh}(t) \in Q_{fh}$, $p_{ph} \in W_{ph}$ such that

$$\begin{aligned}
&\int_{\Omega_f} \frac{\partial \mathbf{u}_{fh}}{\partial t} \cdot \mathbf{v}_{fh} + \int_{\Omega_f} \left((\mathbf{u}_{fh} \cdot \nabla)\mathbf{u}_{fh}\right) \cdot \mathbf{v}_{fh} + \int_{\Omega_f} \frac{1}{\mathrm{Re}_f} \nabla \mathbf{u}_{fh} \cdot \nabla \mathbf{v}_{fh} - \int_{\Omega_f} p_{fh} \nabla \cdot \mathbf{v}_{fh} + \int_{\Gamma} p_{ph} \mathbf{v}_{fh} \cdot \mathbf{n}_f\\
&\quad + \int_{\Gamma} \frac{\mathrm{Gr}_c}{\mathrm{Re}_f} (\mathbf{u}_{fh})_\tau \cdot (\mathbf{v}_{fh})_\tau = 0 \quad \forall \mathbf{v}_{fh} \in \mathbf{V}_{fh},\\
&\int_{\Omega_f} q_{fh} \nabla \cdot \mathbf{u}_{fh} = 0 \quad \forall q_{fh} \in Q_{fh},\\
&\int_{\Omega_p} \mathrm{Gr}_n \nabla p_{ph} \cdot \nabla q_{ph} - \int_{\Gamma} \mathbf{u}_{fh} \cdot \mathbf{n}_f q_{ph} = 0 \quad \forall q_{ph} \in W_{ph},
\end{aligned} \tag{34}$$

with $\mathbf{u}_{fh}(t) = \mathbf{u}^h_{pois}$ on γ_1, $\mathbf{u}_{fh}(t) = \mathbf{0}$ on γ_2 and $\mathbf{u}_{fh}(0) = \mathbf{u}^h_{pois}$ in Ω_f. The discrete velocity $\mathbf{u}^h_{pois}$ is a suitable approximation of $\mathbf{u}_{pois}$ in the finite element space $\mathbf{X}_{fh}$. (The mathematical analysis of the time-dependent NSD problem has been recently carried out in [14].)

In the case of the NSF problem (30), we cannot eliminate the unknown velocity $\mathbf{u}_p$ in Ω_p as done for the Darcy equation. Thus, to write the Galerkin approximation of (30) we should consider a suitable family of inf–sup stable finite element spaces also in the porous domain. Moreover, we should introduce Lagrange multipliers to impose the continuity condition $(30)_5$, following the approach used in [40] to deal with the velocity-pressure formulation of the Darcy problem. However, in our applications we will not use such mixed formulation for the Forchheimer equation, but we will solve only for p_p in Ω_p, as explained in Section 3.3. Thus, we do not discuss here the mixed finite element formulation and we refer the reader to [28,32,44].

In analogous way, we can define the following finite element spaces for the PE approach:

$$\mathbf{X}_h = \left\{\mathbf{v}_h \in \mathcal{C}^0(\overline{\Omega})\colon\ \mathbf{v}_{h|T} \in \left[\mathbb{P}_2(T)\right]^2\ \forall T \in \mathcal{T}_h\right\},$$

$$\mathbf{V}_h = \{\mathbf{v}_h \in \mathbf{X}_h\colon\ \mathbf{v}_h = \mathbf{0} \text{ on } \gamma_1 \cup \gamma_2 \text{ and } \mathbf{v}_h \cdot \mathbf{n} = 0 \text{ on } \delta_1 \cup \delta_2\},$$

$$Q_h = \left\{q_h \in \mathcal{C}^0(\overline{\Omega})\colon\ q_{h|T} \in \mathbb{P}_1(T)\ \forall T \in \mathcal{T}_h\right\}.$$

The Galerkin approximation of (31) reads: find $\mathbf{u}_h(t) \in \mathbf{X}_h$, $p_h \in Q_h$ such that

$$\begin{aligned}
&\int_\Omega \frac{\partial \mathbf{u}_h}{\partial t} \cdot \mathbf{v}_h + \int_\Omega \left((\mathbf{u}_h \cdot \nabla)\mathbf{u}_h\right) \cdot \mathbf{v}_h + \int_\Omega \frac{1}{\mathrm{Re}} \nabla \mathbf{u}_h \cdot \nabla \mathbf{v}_h - \int_\Omega p_h \nabla \cdot \mathbf{v}_h \\
&\quad + \int_\Omega \mathrm{Gr}_v\, \mathbf{u}_h \cdot \mathbf{v}_h + \int_\Omega \mathrm{Gr}_i\, |\mathbf{u}_h| \mathbf{u}_h \cdot \mathbf{v}_h = 0 \quad \forall \mathbf{v}_h \in \mathbf{V}_h, \\
&\int_\Omega q_h \nabla \cdot \mathbf{u}_h = 0 \quad \forall q_h \in Q_h,
\end{aligned} \tag{35}$$

with $\mathbf{u}_h(t) = \mathbf{u}_{pois}^h$ on γ_1, $\mathbf{u}_h(t) = \mathbf{0}$ on γ_2, $\mathbf{u}_h(0) = \mathbf{u}_{pois}^h$ in Ω_f and $\mathbf{u}_h(0) = \mathbf{0}$ in Ω_p. The discrete velocity $\mathbf{u}_{pois}^h$ is a suitable approximation of $\mathbf{u}_{pois}$ in the finite element space $\mathbf{X}_h$.

3.2. Time discretization

To carry out the time discretization we keep in mind our main application: the simulation of the stationary air flow over the porous comfort layer inside a motorbike helmet. Then, since we are interested in the steady state solution, we adopt a first-order implicit Euler scheme with a semi-implicit treatment of the non-linear convective term of the Navier–Stokes equations.

We subdivide the time interval considering a fixed time step Δt: $0 = t^0 < t^1 < \cdots < t^n < t^{n+1} < \cdots$, $t^{n+1} - t^n = \Delta t$, $\forall n \geqslant 0$, and we denote by the upper index n a quantity computed at the time step t^n.

Thus, the discretization in time and space of the coupled NSD problem (34) becomes: for $n \geqslant 0$, find $\mathbf{u}_{fh}^{n+1} \in \mathbf{X}_{fh}$, $p_{fh}^{n+1} \in Q_{fh}$, $p_{ph} \in W_{ph}$ such that

$$\begin{aligned}
&\frac{1}{\Delta t} \int_{\Omega_f} \mathbf{u}_{fh}^{n+1} \cdot \mathbf{v}_{fh} + \int_{\Omega_f} \left((\mathbf{u}_{fh}^n \cdot \nabla)\mathbf{u}_{fh}^{n+1}\right) \cdot \mathbf{v}_{fh} + \int_{\Omega_f} \frac{1}{\mathrm{Re}_f} \nabla \mathbf{u}_{fh}^{n+1} \cdot \nabla \mathbf{v}_{fh} - \int_{\Omega_f} p_{fh}^{n+1} \nabla \cdot \mathbf{v}_{fh} + \int_\Gamma p_{ph} \mathbf{v}_{fh} \cdot \mathbf{n}_f \\
&\quad + \int_\Gamma \frac{\mathrm{Gr}_c}{\mathrm{Re}_f} \left(\mathbf{u}_{fh}^{n+1}\right)_\tau \cdot (\mathbf{v}_{fh})_\tau = \frac{1}{\Delta t} \int_{\Omega_f} \mathbf{u}_{fh}^n \cdot \mathbf{v}_{fh} \quad \forall \mathbf{v}_{fh} \in \mathbf{V}_{fh}, \\
&\int_{\Omega_f} q_{fh} \nabla \cdot \mathbf{u}_{fh}^{n+1} = 0 \quad \forall q_{fh} \in Q_{fh}, \\
&\int_{\Omega_p} \mathrm{Gr}_n\, \nabla p_{ph} \cdot \nabla q_{ph} - \int_\Gamma \mathbf{u}_{fh}^{n+1} \cdot \mathbf{n}_f q_{ph} = 0 \quad \forall q_{ph} \in W_{ph},
\end{aligned} \tag{36}$$

with $\mathbf{u}_{fh}^0 = \mathbf{u}_{pois}^h$ in Ω_f and $\mathbf{u}_{fh}^n = \mathbf{u}_{pois}^h$ on γ_1, $\mathbf{u}_{fh}^n = \mathbf{0}$ on γ_2 for all $n \geqslant 0$.

On the other hand, for the PE model (35) we consider also a semi-implicit treatment of the non-linear Forchheimer correction. Thus, its space–time discretization becomes: find $\mathbf{u}_h^{n+1} \in \mathbf{X}_h$, $p_h^{n+1} \in Q_h$ such that

$$\begin{aligned}
&\frac{1}{\Delta t} \int_\Omega \mathbf{u}_h^{n+1} \cdot \mathbf{v}_h + \int_\Omega \left((\mathbf{u}_h^n \cdot \nabla)\mathbf{u}_h^{n+1}\right) \cdot \mathbf{v}_h + \int_\Omega \frac{1}{\mathrm{Re}} \nabla \mathbf{u}_h^{n+1} \cdot \nabla \mathbf{v}_h - \int_\Omega p_h^{n+1} \nabla \cdot \mathbf{v}_h \\
&\quad + \int_\Omega \mathrm{Gr}_v\, \mathbf{u}_h^{n+1} \cdot \mathbf{v}_h + \int_\Omega \mathrm{Gr}_i\, |\mathbf{u}_h^n| \mathbf{u}_h^{n+1} \cdot \mathbf{v}_h = \frac{1}{\Delta t} \int_\Omega \mathbf{u}_h^n \cdot \mathbf{v}_h \quad \forall \mathbf{v}_h \in \mathbf{V}_h, \\
&\int_\Omega q_h \nabla \cdot \mathbf{u}_h^{n+1} = 0 \quad \forall q_h \in Q_h,
\end{aligned} \tag{37}$$

with $\mathbf{u}_h^0 = \mathbf{u}_{pois}^h$ in Ω_f, $\mathbf{u}_h^0 = \mathbf{0}$ in Ω_p, $\mathbf{u}_h^n = \mathbf{u}_{pois}^h$ on γ_1, $\mathbf{u}_h^n = \mathbf{0}$ on γ_2 for all $n \geqslant 0$.

3.3. An iterative algorithm

To solve the coupled problem (36) we would like to set up an iterative method requiring the alternate solution of the Navier–Stokes equations in Ω_f and of the Darcy equation in Ω_p. To this aim, we consider a domain decomposition approach similar to those studied in [19,21].

Since for our applications we are interested in computing the steady state solution, after discretizing in time we do not perform sub-iterations at each time step, but we adopt the following scheme.

Let φ_h^0 and ψ_h^0 be suitable approximations at the initial time of the pressure p_{ph}^0 and of the normal velocity $\mathbf{u}_{fh}^0 \cdot \mathbf{n}_f$ on Γ, respectively. Moreover, let $0 \leqslant \alpha, \beta \leqslant 1$ be two relaxation parameters. Then, for $n \geqslant 0$

1. find $\mathbf{u}_{fh}^{n+1} \in \mathbf{X}_{fh}$, $p_{fh}^{n+1} \in Q_{fh}$ such that

$$\begin{aligned}
&\frac{1}{\Delta t}\int_{\Omega_f} \mathbf{u}_{fh}^{n+1}\cdot\mathbf{v}_{fh} + \int_{\Omega_f}\left((\mathbf{u}_{fh}^{n}\cdot\nabla)\mathbf{u}_{fh}^{n+1}\right)\cdot\mathbf{v}_{fh} + \int_{\Omega_f}\frac{1}{\mathrm{Re}_f}\nabla\mathbf{u}_{fh}^{n+1}\cdot\nabla\mathbf{v}_{fh} - \int_{\Omega_f} p_{fh}^{n+1}\nabla\cdot\mathbf{v}_{fh} + \int_{\Gamma}\varphi_h^n\mathbf{v}_{fh}\cdot\mathbf{n}_f \\
&\quad + \int_{\Gamma}\frac{\mathrm{Gr}_c}{\mathrm{Re}_f}\left(\mathbf{u}_{fh}^{n+1}\right)_\tau\cdot(\mathbf{v}_{fh})_\tau = \frac{1}{\Delta t}\int_{\Omega_f}\mathbf{u}_{fh}^{n}\cdot\mathbf{v}_{fh} \quad \forall\mathbf{v}_{fh}\in\mathbf{V}_{fh}, \\
&\int_{\Omega_f} q_{fh}\nabla\cdot\mathbf{u}_{fh}^{n+1} = 0 \quad \forall q_{fh}\in Q_{fh}.
\end{aligned} \tag{38}$$

2. Update the normal velocity of the fluid across Γ:

$$\psi_h^{n+1} = (1-\beta)\psi_h^n + \beta\mathbf{u}_{fh}^{n+1}\cdot\mathbf{n}_f \quad \text{on } \Gamma. \tag{39}$$

3. Find $p_{ph}^{n+1} \in W_{ph}$ such that

$$\int_{\Omega_p}\mathrm{Gr}_n\,\nabla p_{ph}^{n+1}\cdot\nabla q_{ph} - \int_{\Gamma}\psi_h^{n+1}q_{ph} = 0 \quad \forall q_{ph}\in W_{ph}. \tag{40}$$

4. Compute the new pressure across Γ:

$$\varphi_h^{n+1} = (1-\alpha)\varphi_h^n + \alpha p_{ph}^{n+1} \quad \text{on } \Gamma. \tag{41}$$

5. Increment n and go back to step 1.

This algorithm requires at each step to solve separately and in a sequential fashion the Navier–Stokes equations in Ω_f and the Darcy equations in Ω_p. Its structure resembles the classical Dirichlet–Neumann method in domain decomposition (see, e.g., [47]). However, notice that here, due to the characteristics of the problems at hand, the conditions imposed on the interface are of Neumann type for both sub-problems.

This approach allows us to easily replace the Darcy model by the Forchheimer equation solving the latter only for p_{ph} at each iteration. Indeed, adopting a semi-implicit treatment of the non-linear term of the Forchheimer equation, instead of (40) we consider the problem: find $p_{ph}^{n+1} \in W_{ph}$ such that

$$\int_{\Omega_p}\frac{\mathrm{Gr}_n}{1+\mathrm{Gr}_f\,|\mathbf{u}_{ph}^n|}\nabla p_{ph}^{n+1}\cdot\nabla q_{ph} - \int_{\Gamma}\psi_h^{n+1}q_{ph} = 0 \quad \forall q_{ph}\in W_{ph}. \tag{42}$$

The velocity in Ω_p at time t^{n+1} can then be recovered by:

$$\mathbf{u}_p^{n+1} = -\frac{\mathrm{Gr}_n}{1+\mathrm{Gr}_f\,|\mathbf{u}_p^n|}\nabla p_p^{n+1} \quad \text{in } \Omega_p. \tag{43}$$

4. Numerical comparison between the different models in a 2D test case

In this section we present some numerical results on a 2D test case using the three models studied in the previous sections.

We consider a 2D computational domain as shown in Fig. 2 to represent an air flow in a channel over a slightly porous tissue. We set $\rho = 1.184\ \mathrm{kg/m^3}$, $\mu = 1.855\cdot 10^{-5}\ \mathrm{Pa\,s}$, $K = 3.71\cdot 10^{-7}\ \mathrm{m^2}$, $\alpha_{BJ} = 1.0$, $C_F = 0.5$. Referring to Fig. 2, our domain has length of 50 mm in the x-direction, height of 4 mm in the fluid domain and of 3 mm in the porous region.

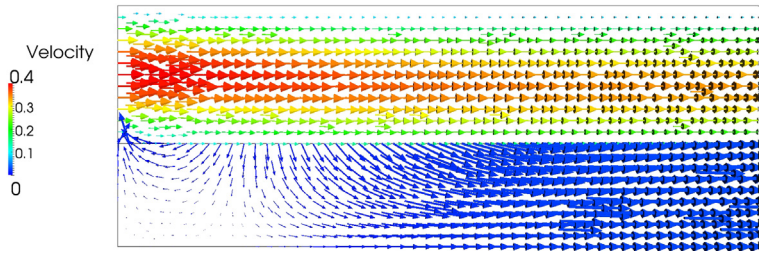

Fig. 4. Vector plot of the steady-state flow field computed with the NSF model (only the first 25 length units in the x-direction are visualized).

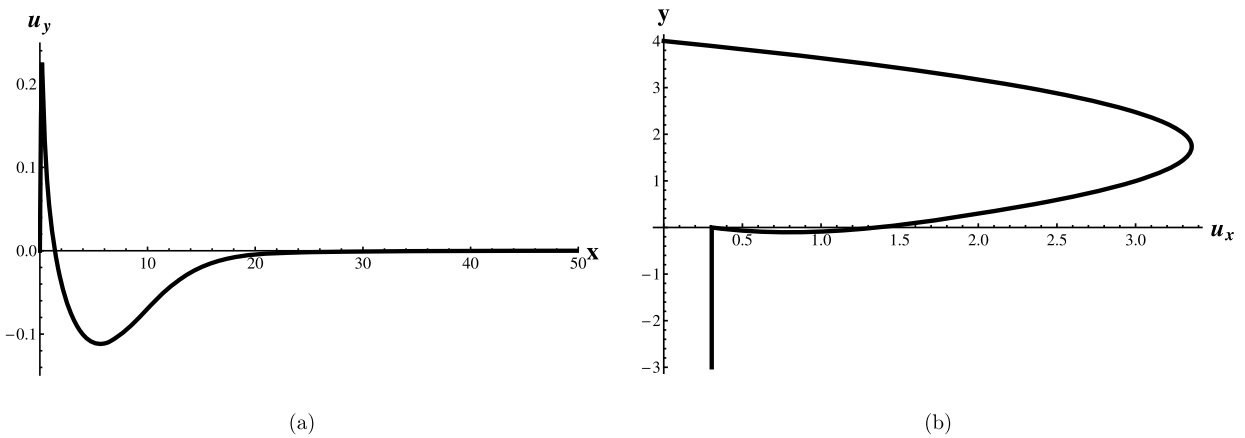

Fig. 5. NSF model: normal velocity through the interface computed with respect to the y-direction (a) and velocity profile at the outlet (b) (i.e., at 50 length units in the x-direction).

As reference characteristic quantities we consider $L = 10^{-3}$ m and $U = 10^{-1}$ m/s. Thus, the dimensionless parameters characterizing the models NSD, NSF and PE are: $\mathrm{Re}_f = 6.38$, $\mathrm{Gr}_n = 2.37$, $\mathrm{Gr}_f = 1.94$, $\mathrm{Gr}_c = 1.64$, $\mathrm{Gr}_v = 0.42$ and $\mathrm{Gr}_i = 0.82$. (The dimensionless domain has dimension of 50 unit lengths in the x-direction and height of 4 and 3 unit lengths in the fluid and in the porous medium regions, respectively.) Notice that in our case it is difficult to quantify Re_p in (4) as the pore size δ is unknown. Boundary conditions are specified as in Section 2.6 and the Poiseuille velocity profile on the inlet boundary γ_1 is $\mathbf{u}_{pois} = (y(4-y), 0)$.

The numerical implementation is carried out in the finite element package freeFEM++ [33], using the multi-frontal algorithms of UMFPACK for solving the local linear systems. The computational grids are uniform, unstructured, conforming on Γ and they are characterized by the adimensional grid parameter $h = 1/N$, N being the number of partitions of each unit length. $\mathbb{P}_2 - \mathbb{P}_1$ finite elements have been used for the spatial discretization.

We consider at first the NSF model with the iterative algorithm of Section 3.3. The NSF model permits to characterize explicitly Γ and to deal with larger Reynolds numbers Re_p in the porous media domain than if the Darcy model is adopted (see [4,42]).

In Fig. 4 we show the finite element solution of the NSF problem at the steady state on a computational mesh with $N = 3$ corresponding to $h = 1/3$ and to about 6500 elements. We can see that the flow suddenly enters the porous medium creating a little recirculation region and then it stabilizes in an almost horizontal flow.

The normal component of the velocity through the interface is plotted in Fig. 5(a), which clearly highlights that the major filtration occurs during the first 15–20 length units. The velocity profile at the outlet (i.e., at 50 length units in the x-direction) represented in Fig. 5(b) shows that the fluid velocity close to the interface is higher than the seepage velocity in the porous medium.

The flow is conserved in the computational domain. Indeed, if we compute the flux on the boundaries:

$$\mathcal{F}_\gamma = \int_{\gamma_1 \cup \gamma_3 \cup \delta_3} \mathbf{u} \cdot \mathbf{n},$$

with obvious choice of notation we have $\mathcal{F}_{\gamma_1} = -10.667$, $\mathcal{F}_{\gamma_3} = 9.285$, $\mathcal{F}_{\delta_3} = \mathcal{F}_\Gamma = 1.382$, so that $\mathcal{F}_\gamma = 0$.

The velocity profile at the outlet can be also evaluated analytically for the NSF coupled problem under the assumption of a fully horizontal flow, that is placing oneself at infinite distance from the inlet. The velocity field in Ω_f becomes $\mathbf{u}_f = (u(y), 0)$ where $u(y)$ is the solution of the boundary value problem:

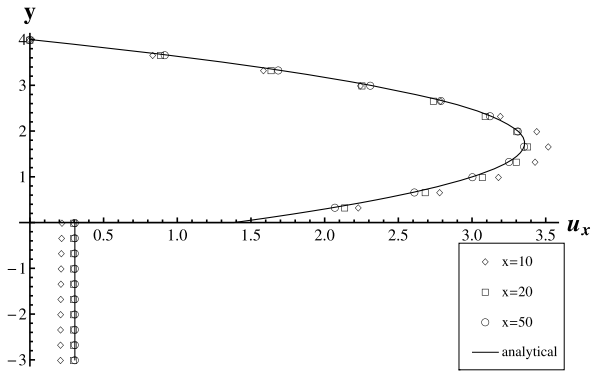

Fig. 6. Comparison between the analytical solution (solid line) and the numerical results obtained with the NSF model on different sections along the x-direction (dots), for the x component of the velocity.

$$-\frac{1}{\mathrm{Re}_f}\frac{d^2u}{dy^2}+\delta p=0 \quad 0\leqslant y\leqslant 4, \tag{44}$$

with the Dirichlet boundary condition on the top boundary:

$$u(4)=0, \tag{45}$$

and with the Robin boundary condition at the contact interface with the porous medium:

$$u'(0)=\mathrm{Gr}_c\, u(0). \tag{46}$$

Here, δp represents the constant value of the pressure drop along the x-direction.

On the other hand, the (constant) horizontal seepage velocity in the porous medium becomes $\mathbf{u}_p=(0,v)$ where v is the solution of the Forchheimer equation for the limit horizontal flow:

$$v+\mathrm{Gr}_f\, v^2+\mathrm{Gr}_n\,\delta p=0. \tag{47}$$

Moreover, we have to impose the flow conservation between the inlet and outlet boundaries:

$$\int_0^4 u_{pois}(y)\,dy=\int_0^4 u(y)\,dy+\int_{-3}^0 v\,dy, \tag{48}$$

u_{pois} being the x-component of $\mathbf{u}_{pois}$.

The solution of (44)–(48) is

$$u(y)=-\frac{D_1\,\mathrm{Re}_f}{2^{14}A_2B_3\,\mathrm{Gr}_f}(y-4)(y+4+4\,\mathrm{Gr}_c\,y), \tag{49}$$

$$v=\frac{1}{2\,\mathrm{Gr}_f}\left(\sqrt{1+\frac{D_1\,\mathrm{Gr}_n}{2^{11}B_3}}-1\right), \tag{50}$$

where $A_1=1+\mathrm{Gr}_c$, $A_2=1+4\,\mathrm{Gr}_c$, $A_3=9+64\,\mathrm{Gr}_f$, $B_1=64A_1A_2A_3\,\mathrm{Re}_f$, $B_2=81A_2^2\,\mathrm{Gr}_n$, $B_3=A_1^2\,\mathrm{Re}_f^2$, $C_1=A_2(2B_1\,\mathrm{Gr}_n+B_2\,\mathrm{Gr}_n+2^{12}B_3)^{1/2}$, $D_1=-9C_1+B_1+B_2$.

In the case that we are considering, we have

$$u(y)=1.38426+2.27264y-0.654677y^2 \quad \text{and} \quad v=0.304974.$$

The computed and the analytical profiles are compared in Fig. 6: as soon as the flow becomes parallel, which occurs near the outlet of the domain (i.e., at 50 length units in the x-direction), the analytical solution coincides with the numerical one. The numerical solution has been computed setting $N=3$.

The effect of the Forchheimer coefficient C_F on the flow is illustrated in Fig. 7, where we can see that the behavior of the flow in the recirculation zone near the inlet is modified as well as the velocity profile at outlet. Moreover, from the physical viewpoint, we remark that as the Forchheimer coefficient raises from 0.0 to 0.5 (its range of variability) the flux filtrating into the porous medium decreases (see Fig. 7(c)).

Let us consider now the NSD model. With the same settings used for the NSF model, we compute the solution of the NSD problem for different values of the permeability K.

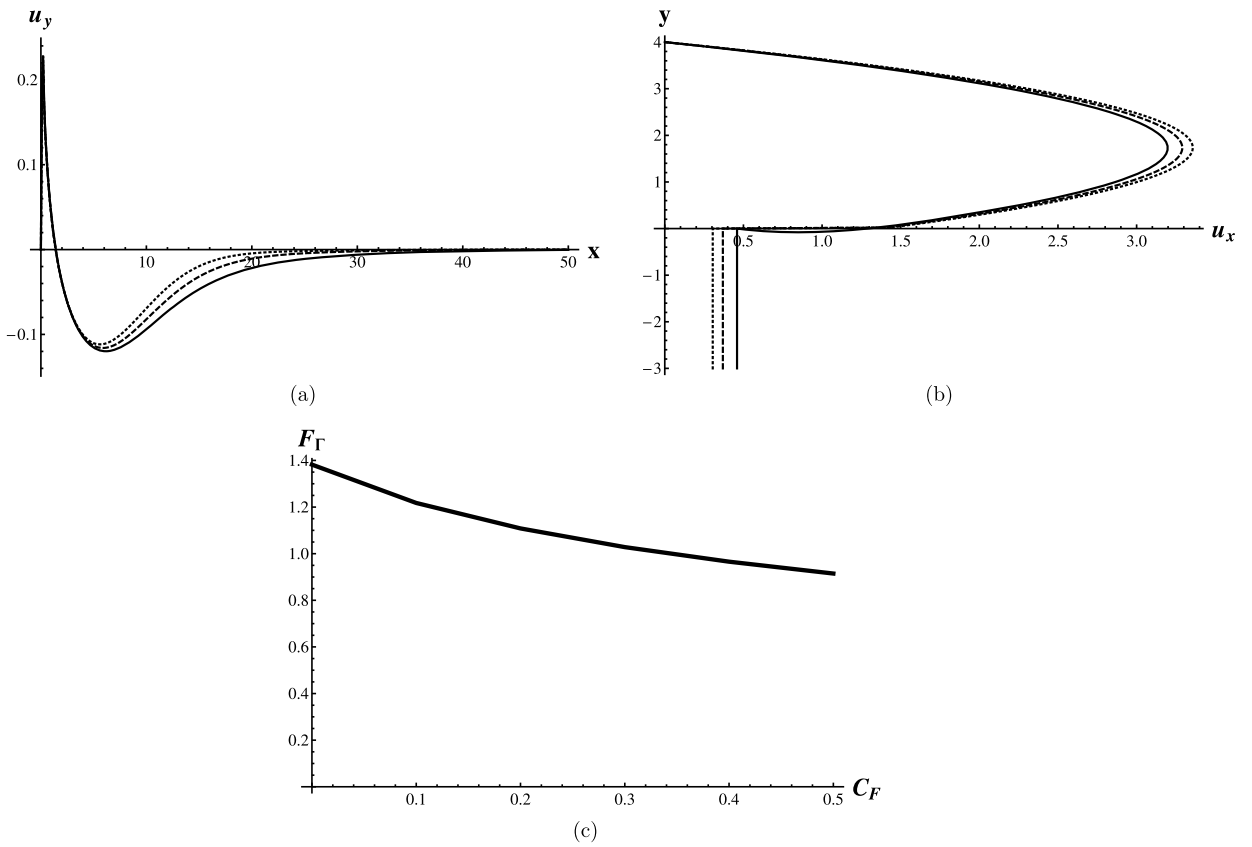

Fig. 7. NSF model: (a) normal component of the velocity across the interface and (b) velocity profile at outlet for values of C_F of 0.0 (solid line), 0.2 (dashed line) and 0.5 (dotted line). (c) Flux entering the porous domain as a function of C_F.

Fig. 8 shows the computed normal velocities and outflow profiles for increasing values of K. As expected, as K grows, more and more flow enters the porous medium (see Fig. 8(c)).

Moreover, for both the NSD and the NSF models, notice that for high values of the permeability the gap between the tangential component of the velocity of the fluid and the seepage velocity across the interface Γ reduces. Thus, Saffman's assumption $\mathbf{u}_p \ll \mathbf{u}_f$ on the interface is no more satisfied, and for large K the original Beavers and Joseph condition (11) cannot be replaced by (13). The difference between the two conditions can be directly seen on the computed velocity profile at the outlet (see Fig. 9).

The values of K used for the simulations reported in Figs. 7(a)–(b) and 8(a)–(b) are chosen to represent a porous medium with high permeability. In correspondence to such values, which are of interest for our target application (see Section 5), we can appreciate the difference between the results computed with two models NSD and NSF.

If the value of the permeability becomes smaller, the results computed with those two models cannot be distinguished as we can see in Fig. 10, where we compare the velocities and fluxes obtained for values of K from 10^{-7} to 10^{-10} m^2. In such cases, it seems not worth using the non-linear Forchheimer model instead of the Darcy one.

We compare now NSD, NSF and PE. As expected, the PE model shows a very smooth transition of the velocity field from Ω_f to the porous medium, in contrast to the jump that characterizes NSD and NSF (see Fig. 11). Looking at the velocity profile obtained by PE, it would be impossible to find out where the porous medium is placed. Thus, this model does not represent correctly the macroscopic physical behavior in the contact area with the porous medium.

However, outside the transition zone, the PE model compares quite well with the others. Indeed, at the outlet of the fluid domain, although the peak velocity is different (since the total flow must be constant), the velocity near the interface is very close to the one given by NSF or NSD. We can then conclude that the velocity profile is quite similar, except in the very first layer of the porous medium.

Observing the normal velocity in Fig. 12, we can see that much more flow enters the porous medium in the case of the PE solver, since the inertial effects are taken in account not only by the Forchheimer term, but also by the inertial term of the Navier–Stokes equations.

Finally, we study the flux $\mathcal{F}_\Gamma$ (or equivalently $\mathcal{F}_{\delta_3}$), analyzing its behavior with respect to the permeability K and the Forchheimer coefficient C_F (in the latter case, we set the permeability to its original value $K = 3.71 \cdot 10^{-7}$ m^2). Fig. 13 gives

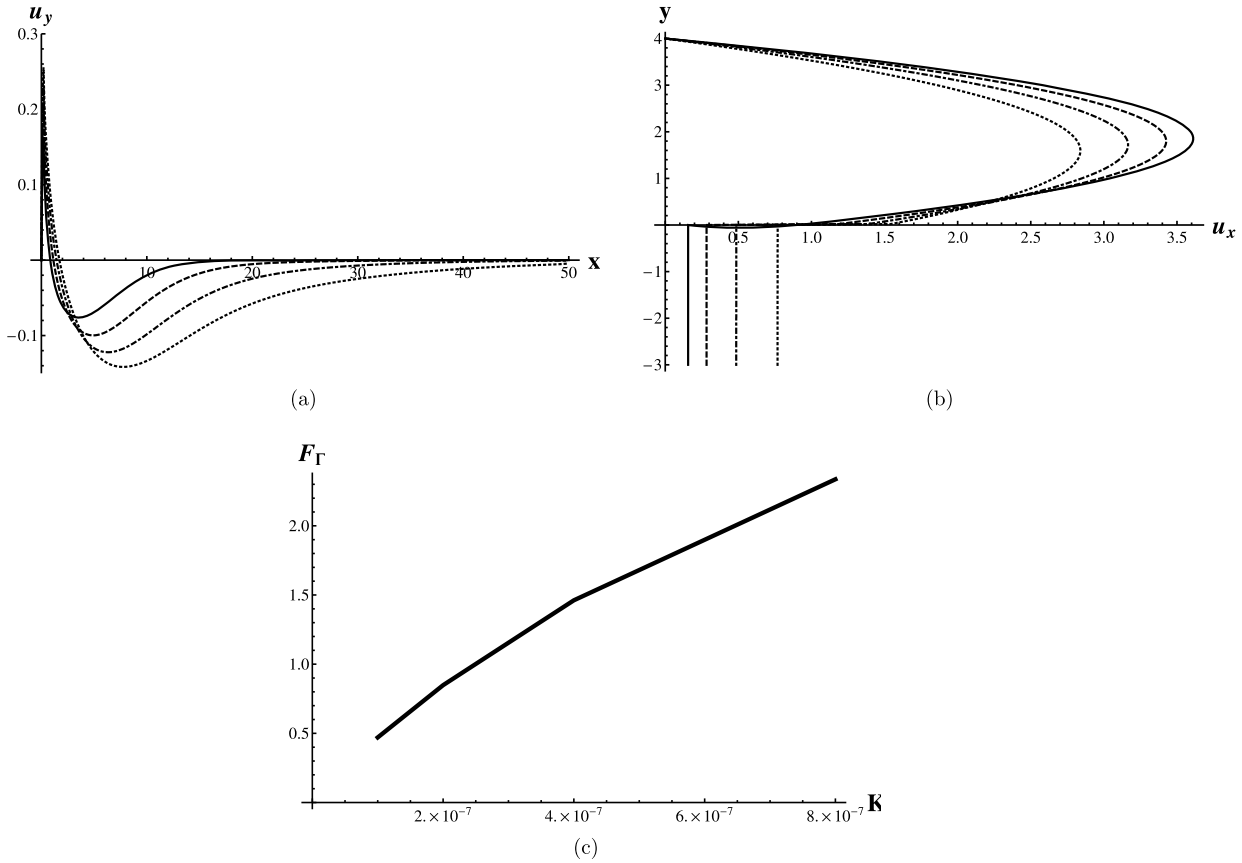

Fig. 8. NSD model: (a) normal component of the velocity across the interface and (b) velocity profile at outlet for values of K equal to 10^{-7} (solid line), $2 \cdot 10^{-7}$ (dashed line), $4 \cdot 10^{-7}$ (dot-dashed line) and $8 \cdot 10^{-7}$ (dotted line). (c) Flux entering the porous domain as a function of K.

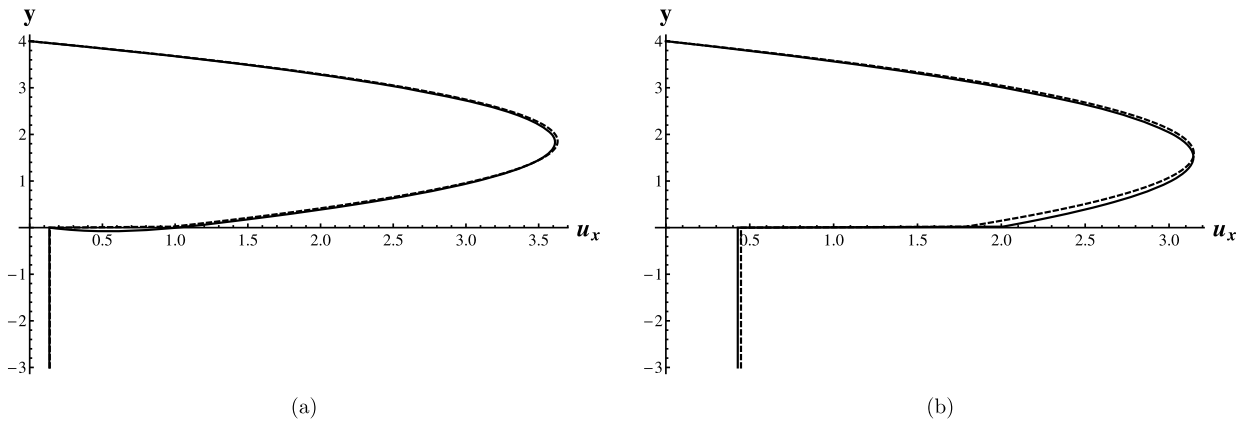

Fig. 9. NSF model ($C_F = 0.5$): comparison between the velocity profile at outlet obtained using the Beavers–Joseph interface condition (solid line) and Beavers–Joseph–Saffman one (dashed line), for a small value of the permeability $K = 10^{-7}$ m^2 (a) and a high one $K = 10^{-6}$ m^2 (b).

a comparison of its trend for the NSF and PE models. Although the values do not match, we can observe that all the curves display the same trends.

Concerning the computational costs, despite its easiness of implementation if compared to NSD and NSF, the PE method is more expensive than the other two. Indeed, PE requires to solve the full Navier–Stokes equations both in Ω_f and Ω_p while NSD and NSF replace them, respectively, by the simpler Darcy or Forchheimer equations in the porous media domain Ω_p.

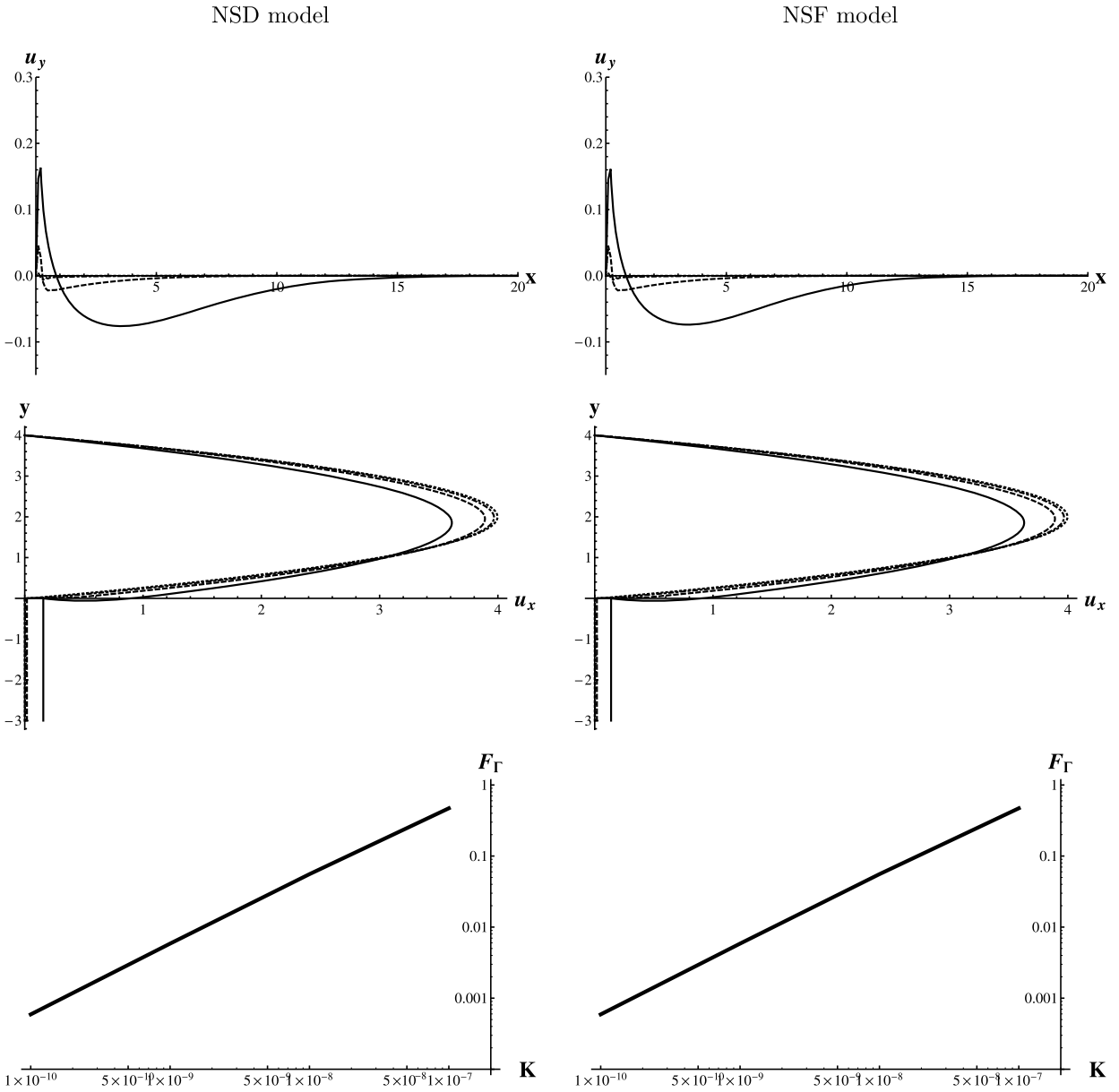

Fig. 10. Comparison between the normal component of the velocity across the interface (top), the velocity profile at outlet (mid) and the flux entering the porous domain (bottom) computed using either the NSD or the NSF model with K equal to 10^{-7} (solid line), 10^{-8} (dashed line), 10^{-9} (dot-dashed line) and 10^{-10} (dotted line).

5. Application to a 3D configuration of internal ventilation of a helmet

In this section we apply the PE approach to study a 3D configuration representing a schematic test case for the real helmet ventilation problem that motivated this work.

The problem of internal ventilation of a motorcycle helmet is associated with the thermal comfort of the rider: a sufficient airflow must be guaranteed to ensure the use of the helmet even in very hot and humid external conditions. For these reasons each helmet has to be equipped with an efficient ventilation system capable of removing as much heat and sweat as possible from the head of the rider. At the moment there is a total lack of fluid-dynamic guidelines for the design of such ventilation systems, which are drawn only according to intuition and experience.

Fig. 14 shows a sample geometry of one of such ventilation systems: a channel dug into the protection layer lets the external air enter inside the helmet, leading it directly above the head. The model includes two porous layers (with different permeabilities) in order to represent the comfort tissue attached to the interior of the helmet and the hair of the rider. The airflow is actually induced by the pressure gap between the inlet and the outlet, which is associated with the external shape

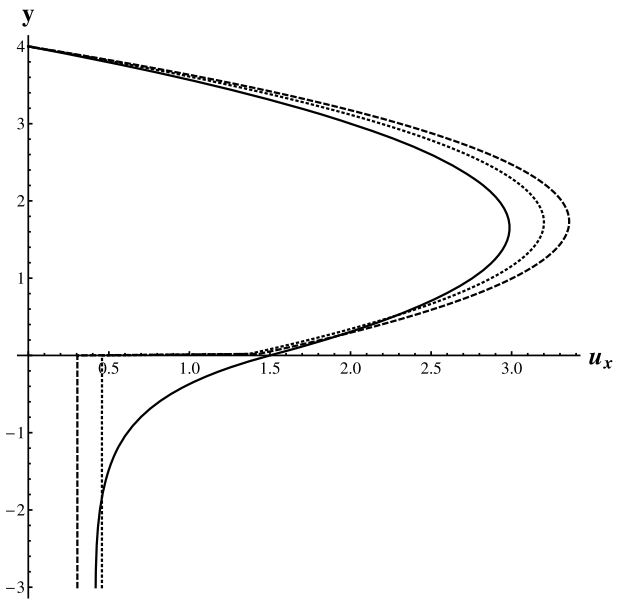

Fig. 11. Velocity profile at outlet: solvers comparison (NSD dotted line, NSF dashed line, PE solid line).

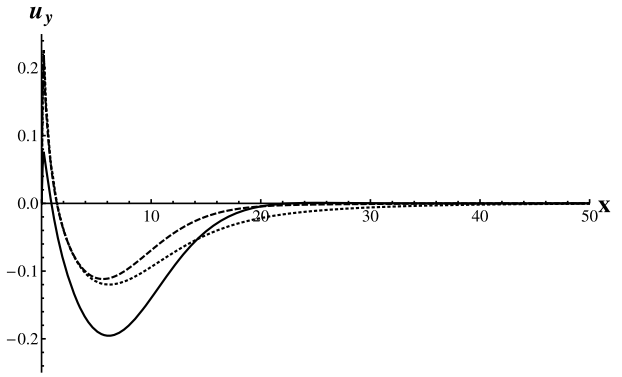

Fig. 12. Normal component of the velocity across the interface: solvers comparison (NSD dotted line, NSF dashed line, PE solid line).

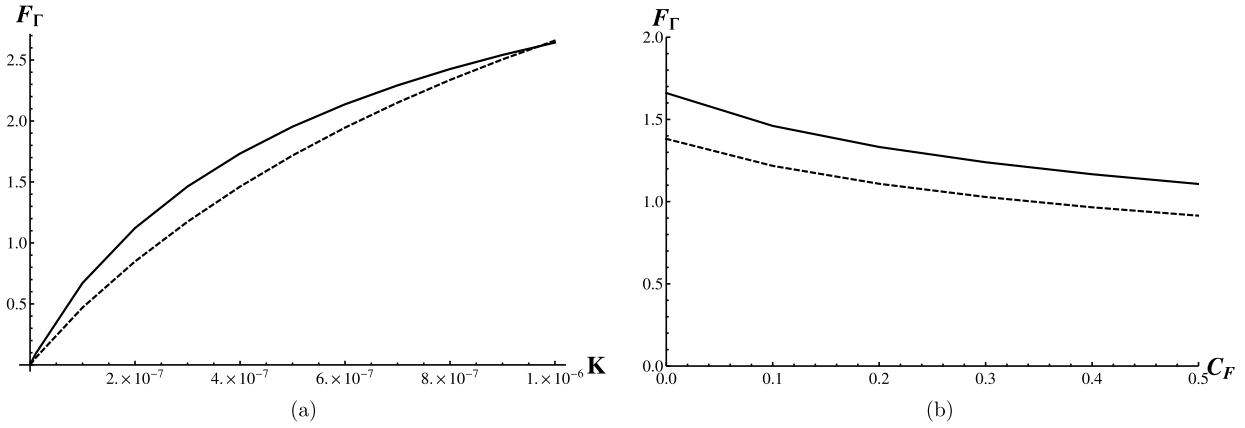

Fig. 13. Trend of the flux across the interface for the NSF model (dashed line) and the PE one (solid line), with respect to the permeability K (a) and the Forchheimer coefficient C_F (b).

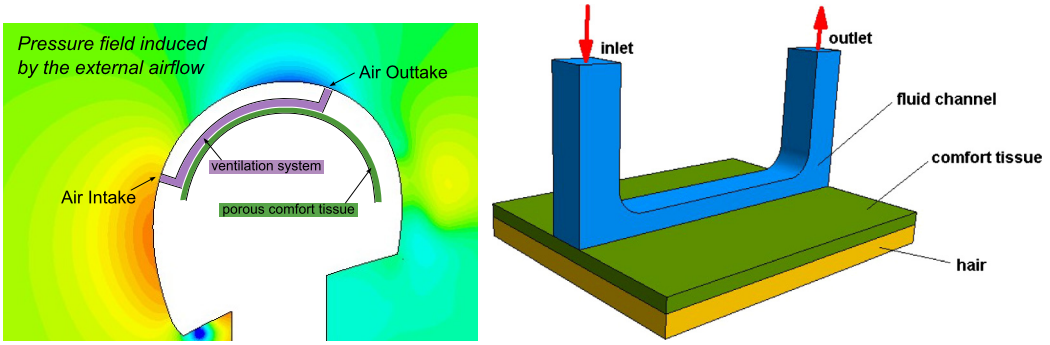

Fig. 14. Schematic representation of an internal ventilation system for a helmet (left) and 3D geometry used in numerical simulations.

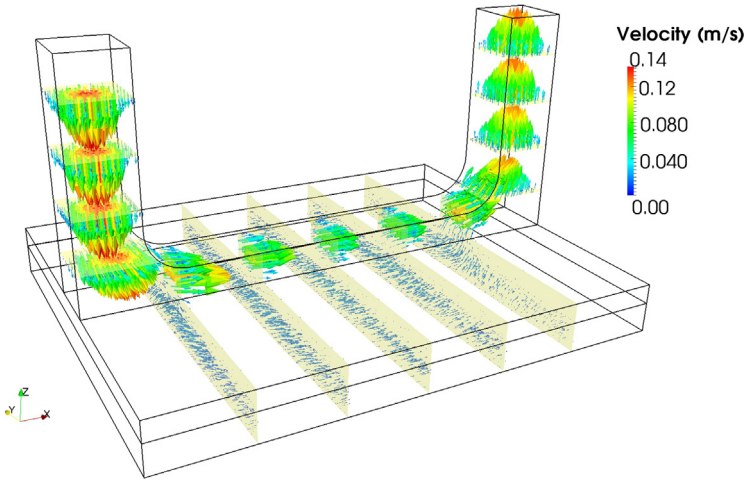

Fig. 15. Velocity field across some vertical and horizontal sections of the domain.

of the helmet as well as with the velocity of the wind. In a real case, such pressure gradient could be obtained either by direct measurements or by external aerodynamics simulation of the cap alone.

Disregarding in a first step the thermal analysis and all the sweat-related issues (we refer the reader to [11]), it is possible to assess the quality of the ventilation system by studying how the airflow is influenced by the geometry of the channels and by the thickness and the physical properties of the porous tissue.

For our simulation, the inlet and outlet channels have a square section of edge 6 mm and their height is 23 mm. The distance between the channels is 50 mm, while the extension of the porous layers in the transversal direction is 40 mm. The porous domain is made of a 2 mm thick comfort tissue with permeability $K_p = 5 \cdot 10^{-8}$ m^2 and Forchheimer coefficient $C_{F,p} = 0.34$, and of the hair layer supposed of 3 mm thickness, with permeability $K_h = 7.5 \cdot 10^{-7}$ m^2 and Forchheimer coefficient $C_{F,h} = 0.5$. (The data used in this simulation have been obtained within a collaboration with an industrial partner. For more details we refer to [16].) An unstructured tetrahedral mesh of about 32 000 elements has been generated using freeFEM++.

We impose a pressure drop of 0.1 Pa between inlet and outlet. We refer to [6,16] on how to include this boundary condition in the weak formulation. On the remaining boundaries we impose a zero airflow condition.

Figs. 15, 16 and 17 show the behavior of the airflow inside the computational domain. In particular, focusing on the medial section, it is possible to see that the seepage velocity is higher on the hair than on the comfort tissue (which has a lower permeability), meaning that the air moves across the latter one and circulates beneath where it encounters a lower resistance.

Finally, we can estimate the mass flow rate of this simple ventilation system by computing the surface integral of the vertical component of the velocity on the inlet (or on the outlet), which turns out to be $2.44 \cdot 10^{-3}$ m^3/s. The mass flow rate could be considered as objective function in an optimization framework aiming at optimizing the physical properties of the porous layer or the shape of the air channels.

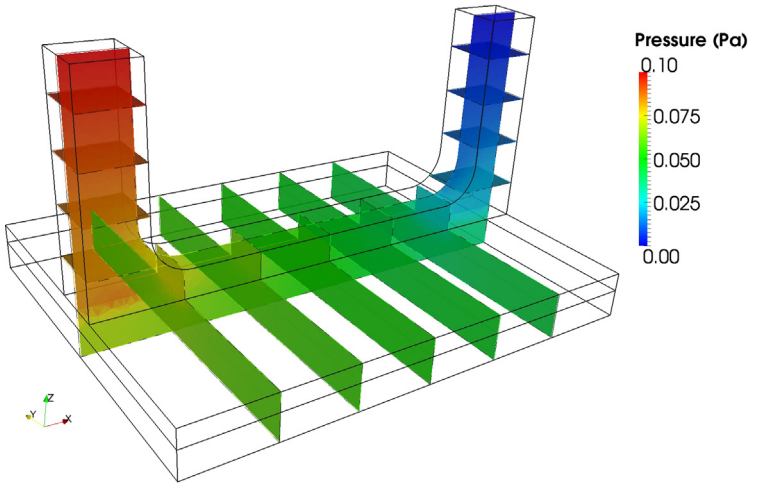

Fig. 16. Pressure field across some vertical and horizontal sections of the domain.

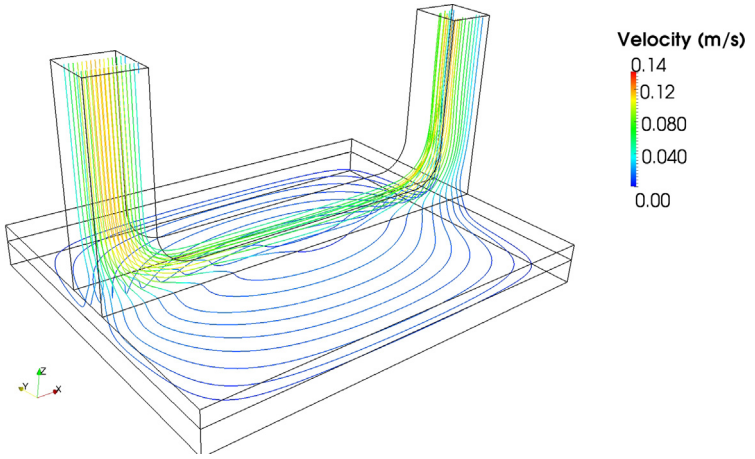

Fig. 17. Streamlines colored by velocity magnitude.

6. Conclusions

We have presented different approaches for modeling incompressible flows in a domain partially occupied by a porous medium. In particular, we have considered models with different equations in the two subregions of the domain coupled via interface conditions (NSD and NSF), and a unified approach (PE) where the presence of the porous region is described by suitable coefficients of the same equation. We have proposed an iterative algorithm to compute the stationary solution of the NSD and NSF models and discussed its implementation. Finally, we have shown an application of the PE method to the computation of the air flow for the internal ventilation of a motorcycle helmet.

We can conclude that, on the one hand, the NSF model allows to represent carefully the physics of the problem since it permits to precisely locate the interface and it features ad-hoc models for each subregion. However, its implementation is rather complex and its solution requires ad-hoc algorithms whose convergence properties may vary sensibly depending on the considered problem.

On the other hand, the penalized model can be straightforwardly implemented in a code already developed for the solution of the Navier–Stokes equations, but it cannot represent correctly the physical behavior of the fluid, especially in the first layers of the porous domain.

From the macroscopic viewpoint the results obtained with these models are not dramatically different. In many engineering applications where a careful description of the flow at the interface between fluid and porous medium is not required, like in the example of internal ventilation of Section 5, the penalization approach can thus provide results similar to those obtained by the coupled methods with less programming effort.

Acknowledgements

The second author acknowledges the partial support of the Marie Curie Career Integration Grant 2011-294229 within the 7th European Community Framework Programme.

References

[1] P. Angot, Analysis of singular perturbations on the Brinkman problem for fictitious domain models of viscous flows, Math. Methods Appl. Sci. 22 (1999) 1395–1412.
[2] Ansys CFX, CFX-Solver: Theory, 2005.
[3] L. Badea, M. Discacciati, A. Quarteroni, Numerical analysis of the Navier–Stokes/Darcy coupling, Numer. Math. 115 (2010) 195–227.
[4] J. Bear, Hydraulics of Groundwater, McGraw–Hill, New York, 1979.
[5] G. Beavers, D. Joseph, Boundary conditions at a naturally permeable wall, J. Fluid Mech. 30 (1967) 197–207.
[6] C. Bègue, C. Conca, F. Murat, O. Pironneau, Les équations de Stokes et de Navier–Stokes avec des conditions aux limites sur la pression, in: Nonlinear Partial Differential Equations and Their Applications. Collège de France Seminar, vol. IX, Paris, 1985–1986, in: Pitman Res. Notes Math. Ser., vol. 181, Longman Sci. Tech., Harlow, 1988, pp. 179–264.
[7] F. Brezzi, M. Fortin, Mixed and Hybrid Finite Element Method, Springer, New York, 1991.
[8] H. Brinkman, A calculation of the viscous force exerted by a flowing fluid on a dense swarm of particles, Appl. Sci. Res. 1 (1949) 27–34.
[9] C. Bruneau, I. Mortazavi, Numerical modelling and passive flow control using porous media, Comput. Fluids 37 (2008) 488–498.
[10] E. Burman, P. Hansbo, A unified stabilized method for Stokes' and Darcy's equations, J. Comput. Appl. Math. 198 (2007) 35–51.
[11] C. Canuto, F. Cimolin, A sweating model for the internal ventilation of a motorcycle helmet, Comput. Fluids 1 (2011) 29–37.
[12] Y. Cao, M. Gunzburger, F. Hua, X. Wang, Coupled Stokes–Darcy model with Beavers–Joseph interface boundary conditions, Commun. Math. Sci. 8 (2010) 1–25.
[13] CD-Adapco, Star-CCM+ User Guide, 2007.
[14] A. Cesmelioglu, V. Girault, B. Rivière, Time-dependent coupling of Navier–Stokes and Darcy flows, Math. Model. Numer. Anal. (2012), in press.
[15] Z. Chen, S. Lyons, G. Qin, Derivation of the Forchheimer law via homogenization, Transp. Porous Media 44 (2001) 325–335.
[16] F. Cimolin, Analysis of the internal ventilation for a motorcycle helmet, Ph.D. thesis, Politecnico di Torino, 2010.
[17] C. D'Angelo, P. Zunino, A finite element method based on weighted interior penalties for heterogeneous incompressible flows, SIAM J. Numer. Anal. 47 (2009) 3990–4020.
[18] H. Darcy, Les Fontaines Publiques de la Ville de Dijon, Dalmont, Paris, 1856.
[19] M. Discacciati, Domain decomposition methods for the coupling of surface and groundwater flows, Ph.D. thesis, Ecole Polytechnique Fédérale de Lausanne, Switzerland, 2004.
[20] M. Discacciati, E. Miglio, A. Quarteroni, Mathematical and numerical models for coupling surface and groundwater flows, Appl. Numer. Math. 43 (2002) 57–74.
[21] M. Discacciati, A. Quarteroni, Navier–Stokes/Darcy coupling: modeling, analysis, and numerical approximation, Rev. Mat. Complut. 22 (2009) 315–426.
[22] H. Ene, E. Sanchez-Palencia, Equations et phénomenès de surface pour l'écoulement dans un modèle de milieu poreux, J. Mécanique 14 (1975) 73–108.
[23] M. Firdaouss, J.L. Guermond, P. Le Quéré, Nonlinear corrections to Darcy's law at low Reynolds numbers, J. Fluid Mech. 343 (1997) 331–350.
[24] Fluent Inc., Fluent User's Guide, 2005.
[25] P. Forchheimer, Wasserbewegung durch Boden, Z. Ver. Deutsch. Ing. 45 (1901) 1782–1788.
[26] J. Galvis, M. Sarkis, Inf–sup for coupling Stokes–Darcy, in: XXV Iberian Latin American Congress in Computational Methods in Engineering, 2005, Recife. Proceedings of the XXV Iberian Latin American Congress in Computational Methods in Engineering, Recife, Brazil, 2004, Universidade Federal de Pernambuco, 2004.
[27] J. Galvis, M. Sarkis, Balancing domain decomposition methods for mortar coupling Stokes–Darcy systems, in: Domain Decomposition Methods in Science and Engineering XVI, in: Lect. Notes Comput. Sci. Eng., vol. 55, Springer, Berlin, 2007, pp. 373–380.
[28] J. Galvis, M. Sarkis, BDD and FETI methods for mortar coupling of Stokes–Darcy, Technical Report Serie A 563, Instituto Nacional de Matemática Pura e Aplicada, Brazil, 2007.
[29] J. Galvis, M. Sarkis, Non-matching mortar discretization analysis for the coupling Stokes–Darcy equations, Electon. Trans. Numer. Anal. 26 (2007) 350–384.
[30] G. Gatica, R. Oyarzúa, F.J. Sayas, Convergence of a family of Galerkin discretizations for the Stokes–Darcy coupled problem, Technical Report 08-11, Departamento de Ingegnería Matemática, Universidad de Conceptión, 2008.
[31] V. Girault, B. Rivière, DG approximation of coupled Navier–Stokes and Darcy equations by Beaver–Joseph–Saffman interface condition, SIAM J. Numer. Anal. 47 (2009) 2052–2089.
[32] V. Girault, M. Wheeler, Numerical discretization of a Darcy–Forchheimer model, Numer. Math. 110 (2008) 161–198.
[33] F. Hecht, O. Pironneau, A. Le Hyaric, K. Ohtsuka, Freefem++ Manual, second ed., 2008.
[34] O. Iliev, V. Laptev, On numerical simulation of flow through oil filters, Comput. Visual. Sci. 6 (2004) 139–146.
[35] O. Iliev, D. Vasileva, On a local refinement solver for coupled flow in plain and porous media, in: Numerical Methods and Applications – 6th International Conference, NMA 2006, Borovets, Bulgaria, August 20–24, 2006, in: Lecture Notes in Computer Science, Springer, Berlin and Heidelberg, 2007, pp. 590–598.
[36] W. Jäger, A. Mikelić, On the boundary conditions at the contact interface between a porous medium and a free fluid, Ann. Scuola Norm. Sup. Pisa Cl. Sci. 23 (1996) 403–465.
[37] W. Jäger, A. Mikelić, On the interface boundary condition of Beavers, Joseph and Saffman, SIAM J. Appl. Math. 60 (2000) 1111–1127.
[38] W. Jäger, A. Mikelić, N. Neuss, Asymptotic analysis of the laminar viscous flow over a porous bed, SIAM J. Sci. Comput. 22 (2001) 2006–2028.
[39] K. Khadra, P. Angot, S. Parneix, J. Caltagirone, Fictitious domain approach for numerical modelling of Navier–Stokes equations, Int. J. Numer. Meth. Fluids 34 (2000) 651–684.
[40] W. Layton, F. Schieweck, I. Yotov, Coupling fluid flow with porous media flow, SIAM J. Numer. Anal. 40 (2003) 2195–2218.
[41] T. Levy, E. Sanchez-Palencia, On the boundary conditions for fluid flow in porous media, Int. J. Engng. Sci. 13 (1975) 923–940.
[42] E. Marušić-Paloka, A. Mikelić, The derivation of a nonlinear filtration law including the inertia effects via homogenization, Nonlinear Anal. 42 (2000) 97–137.
[43] M.C. Néel, Convection forcée en milieu poreux: écarts à la loi de Darcy, C. R. Acad. Sci. Paris, Série IIb 326 (1998) 615–620.
[44] E.J. Park, Mixed finite element methods for generalized Forchheimer flow in porous media, Numer. Methods Partial Differential Equations 21 (2005) 213–228.
[45] L. Payne, B. Straughan, Analysis of the boundary condition at the interface between a viscous fluid and a porous medium and related modelling questions, J. Math. Pures Appl. 77 (1998) 317–354.

[46] A. Quarteroni, A. Valli, Numerical Approximation of Partial Differential Equations, Springer, Berlin, 1994.
[47] A. Quarteroni, A. Valli, Domain Decomposition Methods for Partial Differential Equations, Oxford University Press, New York, 1999.
[48] B. Rivière, I. Yotov, Locally conservative coupling of Stokes and Darcy flows, SIAM J. Numer. Anal. 42 (2005) 1959–1977.
[49] P. Saffman, On the boundary condition at the interface of a porous medium, Stud. Appl. Math. 1 (1971) 93–101.
[50] L. Tartar, Incompressible fluid flow in a porous medium: convergence of the homogenization process, in: E. Sánchez-Palencia, Non-Homogeneous Media and Vibration Theory, in: Lecture Notes in Physics, vol. 127, Springer, Berlin, 1980, pp. 368–377.
[51] J. Urquiza, D. N'Dri, A. Garon, M. Delfour, Coupling Stokes and Darcy equations, Appl. Numer. Math. 58 (2008) 525–538.
[52] K. Vafai, S. Kim, On the limitations of the Brinkman–Forchheimer-extended Darcy equation, Int. J. Heat Fluid Flow 16 (1995) 11–15.
[53] P. Zunino, Mathematical and numerical modeling of mass transfer in the vascular system, Ph.D. thesis, Ecole Polytechnique Fédérale de Lausanne, Switzerland, 2002.